Simultaneous even- and third-order distortion suppression in a microwave photonic link based on orthogonal polarization modulation, balanced detection, and optical sideband filtering

Xiuyou Han,[1,3] Xiang Chen,[2] and Jianping Yao[2,4]

[1]*School of Physics and Optoelectronic Engineering, Dalian University of Technology, Dalian 116024, China*
[2]*Microwave Photonics Research Laboratory, School of Electrical Engineering and Computer Science, University of Ottawa, Ottawa ON K1N 6N5, Canada*
[3]*xyhan@dlut.edu.cn*
[4]*jpyao@eecs.uottawa.ca*

Abstract: A microwave photonic link (MPL) with simultaneous suppression of the even-order and third-order distortions using a polarization modulator (PolM), an optical bandpass filter (OBPF), and a balanced photodetector (BPD) is proposed and experimentally demonstrated. The even-order distortions are suppressed by utilizing orthogonal polarization modulation based on the PolM and balanced differential detection based on the BPD. The third-order distortions (IMD3) are suppressed by optimizing the spectral response of the OBPF with an optimal power ratio between the optical carrier and the sidebands of the phase-modulated signals from the PolM. Since the suppression of the IMD3 is achieved when the MPL is optimized for even-order distortion suppression, the proposed MPL can operate with simultaneous suppression of the even-order and third-order distortions. The proposed MPL is analyzed theoretically and is verified by an experiment. For a two-tone RF signal of f_1 = 10 GHz and f_2 = 19.95 GHz, the spurious-free dynamic range (SFDR2) is enhanced by 23.4 dB for the second harmonic ($2f_1$), and 29.1 and 27.6 dB for the second intermodulation (f_2-f_1 and f_1 + f_2), as compared with a conventional MPL. For a two-tone RF signal of f_1 = 9.95 GHz and f_2 = 10 GHz, the SFDR3 is increased by 13.1 dB as compared with a conventional MPL.

References and links

1. A. Seeds and K. J. Williams, "Microwave photonics," J. Lightwave Technol. **24**(12), 4628–4641 (2006).
2. J. Capmany and D. Novak, "Microwave photonics combines two world," Nat. Photonics **1**(6), 319–330 (2007).
3. J. Yao, "Microwave photonics," J. Lightwave Technol. **27**(3), 314–335 (2009).
4. V. J. Urick, K. J. Williams, and J. D. McKinney, *Fundamentals of Microwave Photonics* (John Wiley & Sons, Inc., Hoboken, 2015).
5. D. Marpaung, "High dynamic range analog photonic links design and implementation," PhD thesis, University of Twente, Netherland (2009).
6. W. K. Burns, G. K. Gopalakrishnan, and R. P. Moeller, "Multi-octave operation of low-biased modulators by balanced detection," IEEE Photonics Technol. Lett. **8**(1), 130–132 (1996).
7. Y. Cui, Y. T. Dai, K. Xu, F. F. Yin, and J. T. Lin, "Multi-octave operation of analogy optical link using parallel intensity modulators," 2013 12th International Conference on Optical Communications & Networks (ICOCN 13'), Chengdu, China, 1–4 (2013).
8. P. S. Devgan, J. F. Diehl, V. J. Urick, C. E. Sunderman, and K. J. Williams, "Even-order harmonic cancellation for off-quadrature biased Mach-Zehnder modulator with improved RF metrics using dual wavelength inputs and dual outputs," Opt. Express **17**(11), 9028–9039 (2009).

9. Y. Cui, K. Xu, Y. T. Dai, and J. L. Lin, "Suppression of second-order harmonic distortion in ROF links utilizing dual-output MZM and balanced detection," 2012 the IEEE International Topical Meeting on Microwave Photonics (MWP 12'), Noordwijk, Netherland, 103–106 (2012).
10. Q. Lin, Z. Z. Ying, and G. Wei, "Design of a feedback predistortion linear power amplifier," Microw. J. **48**(5), 232–241 (2005).
11. B. Hraimel and X. Zhang, "Low-cost broadband predistortion-linearized single-drive x-cut Mach-Zehnder modulator for radio-over-fiber system," IEEE Photonics Technol. Lett. **24**(18), 1571–1573 (2012).
12. M. L. Farwell, W. S. C. Chang, and D. R. Huber, "Increased linear dynamic range by low biasing the Mach–Zehnder modulator," IEEE Photonics Technol. Lett. **5**(7), 779–782 (1993).
13. S. K. Korotky and R. M. DeRidder, "Dual parallel modulation schemes for low-distortion analog optical transmission," IEEE J. Sel. Areas Comm. **8**(7), 1377–1381 (1990).
14. J. Dai, K. Xu, R. M. Duan, Y. Cui, J. Wu, and J. T. Lin, "Optical linearization for intensity-modulated analog links employing equivalent incoherent combination technique," 2011 the IEEE International Topical Meeting on Microwave Photonics (MWP 11'), Singapore, 230–233 (2011).
15. M. Huang, J. Fu, and S. Pan, "Linearized analog photonic links based on a dual-parallel polarization modulator," Opt. Lett. **37**(11), 1823–1825 (2012).
16. X. Chen, W. Li, and J. P. Yao, "Microwave photonic link with improved dynamic range using a polarization modulator," IEEE Photonics Technol. Lett. **25**(14), 1373–1376 (2013).
17. W. Li and J. Yao, "Dynamic range improvement of a microwave photonic link based on bi-directional use of a polarization modulator in a Sagnac loop," Opt. Express **21**(13), 15692–15697 (2013).
18. X. Chen, W. Li, and J. P. Yao, "Dynamic range enhancement for a microwave photonic link based on a polarization modulator," IEEE Trans. Microw. Theory Tech. **63**(7), 2384–2389 (2015).
19. E. Ackerman, "Broad-band linearization of a Mach-Zehnder electrooptic modulator," IEEE Trans. Microw. Theory Tech. **47**(12), 2271–2279 (1999).
20. J. D. Bull, N. A. F. Jaeger, H. Kato, M. Fairburn, A. Reid, and P. Ghanipour, "40 GHz electro-optic polarization modulator for fiber optic communications systems," Proc. SPIE **5577**(1), 133–143 (2004).
21. C. Lim, M. Attygalle, A. Nirmalathas, D. Novak, and R. Waterhouse, "Analysis of optical carrier-to-sideband ratio for improving transmission performance in fiber-radio links," IEEE Trans. Microw. Theory Tech. **54**(5), 2181–2187 (2006).
22. X. Y. Han, E. M. Xu, and J. P. Yao, "Tunable single bandpass microwave photonic filter with an improved dynamic range," IEEE Photonics Technol. Lett. **28**(1), 11–14 (2016).
23. J. T. Willits, A. M. Weiner, and S. T. Cundiff, "Line-by-line pulse shaping with spectral resolution below 890 MHz," Opt. Express **20**(3), 3110–3117 (2012).
24. E. Rouvalis, F. N. Baynes, X. J. Xie, K. J. Li, Q. G. Zhou, F. Quinlan, T. M. Fortier, S. A. Diddams, A. G. Steffan, A. Beling, and J. C. Campbell, "High-power and high-linearity photodetector modules for microwave photonic applications," J. Lightwave Technol. **32**(20), 3810–3816 (2014).
25. L. Zhuang, M. Hoekman, C. Taddei, A. Leinse, R. G. Heideman, A. Hulzinga, J. Verpoorte, R. M. Oldenbeuving, P. W. van Dijk, K.-J. Boller, and C. G. H. Roeloffzen, "On-chip microwave photonic beamformer circuits operating with phase modulation and direct detection," Opt. Express **22**(14), 17079–17091 (2014).

1. Introduction

Microwave photonic links (MPLs) have been used for various applications such as antenna remoting, phased array beamforming, and wireless access networks, due to the advantages such as very low insertion loss, ultra-broad bandwidth, and high immunity to EMI [1–3]. In general, an MPL with a large spurious-free dynamic range (SFDR) over a broad bandwidth is desired, especially for applications where the electromagnetic environment is complicated, including signal-rich military environments [4]. There are mainly two nonlinear distortions in an MPL [5], the even-order distortions including the second harmonic distortion (SHD) and the second intermodulation distortion (IMD2) which limits MPLs to single-octave applications, and the odd-order distortions including primarily the third-order distortion (IMD3) which degrades the microwave signal power accommodating capacity. A number of approaches have been proposed and demonstrated to reduce either the even-order or the odd-order distortions, but few approaches have been proposed to reduce the two distortions simultaneously.

To eliminate the even-order distortions, one may use two Mach-Zehnder modulators (MZMs) biased symmetrically at the opposite quadrature points. By detecting the optical signals at a balanced photodetector (BPD), the even-order distortion terms can be cancelled [6]. The major limitation of the approach is that the two MZMs are connected via two separate fibers before the modulated optical signals are detected at the BPD, since the lengths of the two fibers must be controlled to be identical, it may not be suitable for long distance application. To avoid using two fibers, an approach based on polarization multiplexing was proposed [7]. By multiplexing two orthogonally polarized optical signals and transmit them in

a single fiber, a second fiber is not needed. For the approaches in [6] and [7], two matched MZMs are needed, which makes the system complicated. A simpler approach is to utilize a single dual-output MZM with dual optical inputs and dual optical outputs [8]. Since the transfer function of a MZM is wavelength dependent, by choosing the two wavelengths with a proper wavelength spacing, the bias points for the two wavelengths can be controlled at the opposite quadrature points. Again, the approach is complicated due to the use of two optical wavelengths. To avoid using two wavelengths, polarization multiplexing may be used. In [9], two complementarily modulated and polarization multiplexed optical signals generated by a dual-output MZM are generated. The complementarity is achieved using a 180° electrical hybrid to produce two complementary microwave signals to apply to the MZM via the two input ports. Of course, the bandwidth of the electrical hybrid will limit the bandwidth of the MPL. All the MPLs reported in [6–9] are able to operate with significantly reduced even-order distortions, but the odd-order distortions are still there which will affect the microwave signal power accommodating capacity of the MPLs.

To eliminate the odd-order distortions, primarily the IMD3, several techniques have been proposed, including those implemented in the electrical domain and the optical domain. Compared with the pre-distortion techniques in the electrical domain [10, 11], the bandwidth can be significantly increased when linearization is implemented in the optical domain. In [12], the SFDR was increased by partially suppressing the optical carrier which was done by lowering the bias point of the MZM to reduce the noise floor of the MPL (to reduce the shot noise at the PD), but the IMD3 was not reduced. In addition, the even-order distortions would be increased because of the increased nonlinearity when lowering the bias point of the MZM. To reduce the IMD3, one may linearize an MPL using two parallel MZMs [13, 14] or polarization modulators (PolMs) [15], where a main modulation path and an auxiliary modulation path were constructed to generate two complementary IMD3 terms, which could be fully cancelled at a PD. Since two MZMs or PolMs are used, the systems are more complicated and costly. We have recently proposed a simplified solution using a single PolM [16–18] that could operate equivalently as two MZMs, which greatly decrease the complexity and cost. Again, the MPLs reported in [12–18] are able to operate with a significantly reduced IMD3, but the even-order distortions are still there or even increased, which may limit the MPLs for single-octave applications only.

A few approaches have been proposed to reduce simultaneously the second-order and third-order distortions. In [19], an MPL using two optical sources with a large wavelength difference and a single MZM was proposed, in which the MZM was biased at the opposite transmission points due to the wavelength-dependent transmission function of the MZM. Both the second-order and third-order distortions were minimized by a precise control of the bias points and the ratio between the optical powers of the two wavelengths. Since the minimization of the second-order and third-order distortions will also lead to a partial cancellation of the fundamental signal, the link loss is high. In addition, the power ratio and the locations of the bias points must be precisely controlled, which make the system very complicated.

In this paper, we propose and experimentally demonstrate a simple and novel approach to implementing an MPL with simultaneously suppressed even-order and third-order distortions. The proposed MPL consists of a single-wavelength light source, a single PolM, an optical bandpass filter (OBPF), an erbium-doped fiber amplifier (EDFA), a polarization beam splitter (PBS), and a BPD. The key device in the MPL is the PolM, which is a special phase modulator that supports complementary phase modulations along the two principal axes [20]. In the MPL, the polarization direction of the optical carrier from the light source is controlled to have an angle of 45° relative to one principle axis of the PolM, thus the incident light wave is projected equally to the two principal axes, and two complementarily phase-modulated optical signals that are orthogonally polarized are generated at the output of the PolM. The phase-modulated optical signals are sent to the OBPF to suppress the left sidebands, to generate two complementarily modulated single-sideband with carrier (SSB + C) signals. By detecting the two SSB + C signals at the BPD (differential detection), the even-order

distortions are fully cancelled. On the other hand, the IMD3 is minimized by optimizing the spectral response of the OBPF to make the powers of the optical carrier and the sidebands to have an optimum ratio. Since the suppression of the IMD3 is achieved independently at each PD of the BPD, namely, in the two orthogonal polarization transmission links, the proposed MPL can operate with simultaneous suppression of the even-order and third-order distortions.

The proposed MPL is analyzed theoretically and is verified by an experiment. For a two-tone microwave signal of $f_1 = 10$ GHz and $f_2 = 19.95$ GHz, an increase in the SFDR2 by 23.4 dB for the SHD ($2f_1$), and 29.1 and 27.6 dB for the second intermodulations (f_2-f_1 and $f_1 + f_2$) is demonstrated, as compared with a conventional MPL operating under the same conditions. For a two-tone microwave signal of $f_1 = 9.95$ GHz and $f_2 = 10$ GHz, an increase in the SFDR3 by 13.1 dB is achieved by optimizing the spectral response of the OBPF.

2. Theory

The schematic of the proposed MPL is shown in Fig. 1. The light wave from a tunable laser source (TLS) is sent to a PolM via a polarization controller (PC1). PC1 is used to align the polarization direction of the light wave with an angle of 45° relative to one principal axis of the PolM. The PolM is a special phase modulator that supports phase modulations along the two principal axes with opposite modulation indices [20]. An RF signal is fed to the PolM via the RF port. The phase-modulated optical signals along the two orthogonal principle axes of the PolM are sent to an optical bandpass filter (OBPF), where the left sidebands of the PM signals are suppressed and two SSB + C signals are obtained. After being amplified by an erbium-doped fiber amplifier (EDFA), the SSB + C signals are sent to a polarization beam splitter (PBS) via the second polarization controller (PC2), which is used to align the two polarization directions of the orthogonal SSB + C signals along the two principle axes of the PBS. The polarization-demultiplexed SSB + C signals from the PBS are applied to the BPD through its upper and lower optical ports. Two electrical signals are generated at the outputs of the two photodetectors (PD1 and PD2) inside the BPD and then combined to get a differential output.
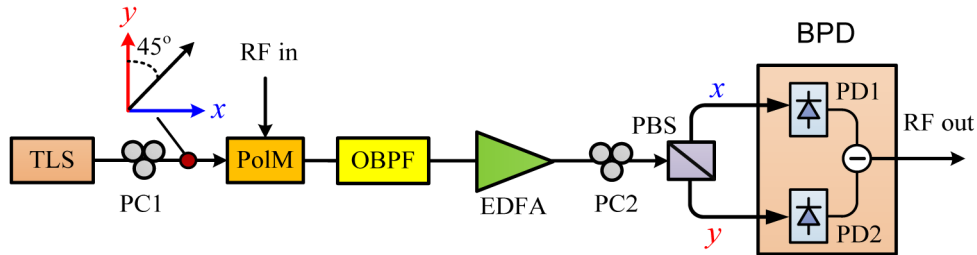
Fig. 1. The schematic of the proposed MPL. TLS: tunable laser source, PolM: polarization modulator, OBPF: optical bandpass filter, EDFA: erbium-doped fiber amplifier, PC: polarization controller, PBS: polarization beam splitter, PD: photodetector, BPD: balanced photodetector.

2.1 Even-order distortion suppression

Assuming two RF signals with two angular frequencies of ω_1 and ω_2 are combined through a 3-dB electrical combiner and fed to the PolM. The electrical fields of the phase-modulated optical signals along the two orthogonal principle axes of the PolM can be expressed as

$$E_{out,PolM,x}(t) = \frac{E_0}{\sqrt{2}} e^{j\omega_c t} e^{j(m_1 \cos\omega_1 t + m_2 \cos\omega_2 t)} \tag{1}$$

$$E_{out,PolM,y}(t) = \frac{E_0}{\sqrt{2}} e^{j\omega_c t} e^{-j(m_1 \cos\omega_1 t + m_2 \cos\omega_2 t)} \tag{2}$$

where E_0 is the amplitude of the electrical field of the input optical carrier, $m_i = \pi V_i/V_\pi$ ($i = 1$, 2) is the modulation index, V_i is the amplitude of the input RF signal, V_π is the half wave voltage of the PolM.

By the Jacobi-Anger expansion (1) and (2) can be rewritten as

$$E_{out,PolM,x}(t) = \frac{E_0}{\sqrt{2}} e^{j\omega_c t} \sum_{k=-\infty}^{+\infty} \sum_{l=-\infty}^{+\infty} J_k(m_1) J_l(m_2) e^{j\left[k\omega_1 t + l\omega_2 t + (k+l)\frac{\pi}{2}\right]} \tag{3}$$

$$E_{out,PolM,y}(t) = \frac{E_0}{\sqrt{2}} e^{j\omega_c t} \sum_{k=-\infty}^{+\infty} \sum_{l=-\infty}^{+\infty} J_k(m_1) J_l(m_2) e^{j\left[k\omega_1 t + l\omega_2 t + (k+l)\frac{3\pi}{2}\right]} \tag{4}$$

where $J_k(m_1)$ and $J_l(m_2)$ are the Bessel functions of the first kind. The SSB + C signals are obtained at the output of the OBPF by suppressing the left sidebands of the phase-modulated signals. The electrical fields of the SSB + C signals can be expressed as

$$E_{out,OBPF,x}(t) = \frac{E_0}{\sqrt{2}} e^{j\omega_c t} \sum_{k=-\infty}^{+\infty} \sum_{l=-\infty}^{+\infty} J_k(m_1) J_l(m_2) \sqrt{R(\omega_c + k\omega_1 + l\omega_2)} e^{j\left[k\omega_1 t + l\omega_2 t + (k+l)\frac{\pi}{2}\right]} \tag{5}$$

$$E_{out,OBPF,y}(t) = \frac{E_0}{\sqrt{2}} e^{j\omega_c t} \sum_{k=-\infty}^{+\infty} \sum_{l=-\infty}^{+\infty} J_k(m_1) J_l(m_2) \sqrt{R(\omega_c + k\omega_1 + l\omega_2)} e^{j\left[k\omega_1 t + l\omega_2 t + (k+l)\frac{3\pi}{2}\right]} \tag{6}$$

where $R(\omega)$ is the power spectral response of the OBPF. The SSB + C signals are amplified by the EDFA and demultiplexed by the PBS. The two SSB + C signals at the outputs of the PBS are expressed as

$$E_{out,PBS,x}(t) = \frac{E_0}{\sqrt{2}} e^{j\omega_c t} \sum_{k=-\infty}^{+\infty} \sum_{l=-\infty}^{+\infty} J_k(m_1) J_l(m_2) \sqrt{R(\omega_c + k\omega_1 + l\omega_2)} \sqrt{G} e^{j\left[k\omega_1 t + l\omega_2 t + (k+l)\frac{\pi}{2}\right]} \tag{7}$$

$$E_{out,PBS,y}(t) = \frac{E_0}{\sqrt{2}} e^{j\omega_c t} \sum_{k=-\infty}^{+\infty} \sum_{l=-\infty}^{+\infty} J_k(m_1) J_l(m_2) \sqrt{R(\omega_c + k\omega_1 + l\omega_2)} \sqrt{G} e^{j\left[k\omega_1 t + l\omega_2 t + (k+l)\frac{3\pi}{2}\right]} \tag{8}$$

where G is the power gain coefficient of the EDFA. Optical to electrical conversion is conducted at PD1 and PD2 and the two electrical signals at the outputs of PD1 and PD2 are expressed as

$$
\begin{aligned}
i_1(t) &= E_{out,PBS,x}(t) \cdot E^*_{out,PBS,x}(t) \\
&= \frac{|E_0|^2}{2} \sum_{k=-\infty}^{+\infty} \sum_{l=-\infty}^{+\infty} \sum_{p=-\infty}^{+\infty} \sum_{q=-\infty}^{+\infty} \left\{ \begin{array}{l} J_k(m_1) J_l(m_2) J_p(m_1) J_q(m_2) \sqrt{R(\omega_c + k\omega_1 + l\omega_2)} \\ \cdot \sqrt{R(\omega_c + p\omega_1 + q\omega_2)} G e^{j\left[(k-p)\omega_1 t + (l-q)\omega_2 t + (k+l-p-q)\frac{\pi}{2}\right]} \end{array} \right\} \\
&= \frac{|E_0|^2}{2} \sum_{k=-\infty}^{+\infty} \sum_{l=-\infty}^{+\infty} \sum_{p=-\infty}^{+\infty} \sum_{q=-\infty}^{+\infty} \left\{ \begin{array}{l} J_k(m_1) J_l(m_2) J_p(m_1) J_q(m_2) \sqrt{R(\omega_c + k\omega_1 + l\omega_2)} \\ \cdot \sqrt{R(\omega_c + p\omega_1 + q\omega_2)} G e^{j\left[(k-p)\omega_1 t + (l-q)\omega_2 t\right]} \\ \cdot \left\{ \begin{array}{ll} (-1)^N, & k-p+l-q = 2N \\ (-1)^N e^{j\frac{\pi}{2}}, & k-p+l-q = 2N+1 \end{array} \right. \end{array} \right\}
\end{aligned} \tag{9}
$$

$$k+l \geq 0,\ p+q \geq 0,\ N = 0 \pm 1, \pm 2, \cdots$$

$$i_2(t) = E_{out,PBS,y}(t) \cdot E^*_{out,PBS,y}(t)$$

$$= \frac{|E_0|^2}{2} \sum_{k=-\infty}^{+\infty} \sum_{l=-\infty}^{+\infty} \sum_{p=-\infty}^{+\infty} \sum_{q=-\infty}^{+\infty} \left\{ \begin{array}{l} J_k(m_1) J_l(m_2) J_p(m_1) J_q(m_2) \sqrt{R(\omega_c + k\omega_1 + l\omega_2)} \\ \cdot \sqrt{R(\omega_c + p\omega_1 + q\omega_2)} G e^{j\left[(k-p)\omega_1 t + (l-q)\omega_2 t + (k+l-p-q)\frac{3\pi}{2} \right]} \end{array} \right\}$$

$$= \frac{|E_0|^2}{2} \sum_{k=-\infty}^{+\infty} \sum_{l=-\infty}^{+\infty} \sum_{p=-\infty}^{+\infty} \sum_{q=-\infty}^{+\infty} \left\{ \begin{array}{l} J_k(m_1) J_l(m_2) J_p(m_1) J_q(m_2) \sqrt{R(\omega_c + k\omega_1 + l\omega_2)} \\ \cdot \sqrt{R(\omega_c + p\omega_1 + q\omega_2)} G e^{j[(k-p)\omega_1 t + (l-q)\omega_2 t]} \\ \cdot \left\{ \begin{array}{ll} (-1)^N, & k-p+l-q = 2N \\ -(-1)^N e^{j\frac{\pi}{2}}, & k-p+l-q = 2N+1 \end{array} \right. \end{array} \right\} \quad (10)$$

$$k+l \ge 0, \ p+q \ge 0, \ N = 0 \pm 1, \pm 2, \cdots$$

A differential signal from the BPD is obtained and can be expressed as

$$i(t) = i_1(t) - i_2(t)$$

$$= \left\{ \begin{array}{ll} 0, & k-p+l-q = 2N \\ |E_0|^2 \sum_{k=-\infty}^{+\infty} \sum_{l=-\infty}^{+\infty} \sum_{p=-\infty}^{+\infty} \sum_{q=-\infty}^{+\infty} \left\{ \begin{array}{l} J_k(m_1) J_l(m_2) J_p(m_1) J_q(m_2) \\ \cdot \sqrt{R(\omega_c + k\omega_1 + l\omega_2)} \\ \cdot \sqrt{R(\omega_c + p\omega_1 + q\omega_2)} G \\ \cdot e^{j[(k-p)\omega_1 t + (l-q)\omega_2 t]} (-1)^N e^{j\frac{\pi}{2}} \end{array} \right\}, & k-p+l-q = 2N+1 \end{array} \right. \quad (11)$$

$$k+l \ge 0, \ p+q \ge 0, \ N = 0 \pm 1, \pm 2, \cdots$$

From (11), it can be seen that all the even-order frequency terms, namely, $\omega = (k-p)\omega_1 + (l-q)\omega_2$, $k-p + l-q = 2N$, $N = 0, \pm 1, \pm 2, \cdots$, are cancelled due to the differential detection at the BPD. As a result, all the even-order distortions are fully eliminated.

2.2 IMD3 suppression

In the proposed MPL, the OBPF is utilized to get the SSB + C signals by suppressing the left sidebands of the phase-modulated signals. Here, we consider the zero-, first- and second-order terms, say $k, l, p, q = 0, \pm 1, \pm 2$, with the condition of the output signal from the BPD,

$$k - p + l - q = 2N + 1, \quad N = 0, \pm 1, \pm 2 \quad (12)$$

Figure 2 shows the spectral components for the signals from the OBPF along the *x* and *y* polarization directions of the PolM when the zero-, first- and second-order terms are considered. The spectral response of the OBPF that functions to suppress the left sidebands of the phase-modulated signals to generate the SSB + C signals is also plotted. The SSB + C signals along the *x* and *y* polarization directions are demultiplexed by the PBS and fed to the BPD through its two optical input ports. Upon detection at the BPD, the fundamental as well as the IMD3 components are generated due to the beating between the frequency components from the OBPF. Tables 1 and 2 give the coefficients of the fundamental components (ω_1 and ω_2) and the IMD3 components ($2\omega_1-\omega_2$ and $2\omega_2-\omega_1$), respectively.
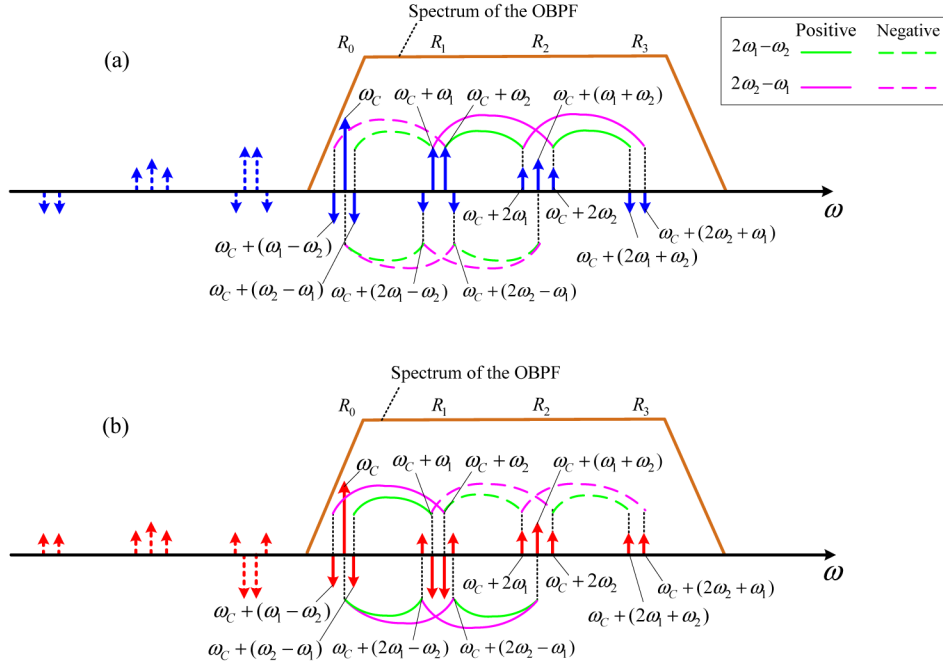
Fig. 2. The spectral components of the orthogonally polarized phase-modulated signals at the output from the OBPF. (a) *x* polarization and (b) *y* polarization. The solid and dash arc lines denote the generation of the positive and negative IMD3 components, respectively, during the optical to electrical conversion at the PDs in the BPD.

According to Table 2, the coefficients for the IMD3 components, $2\omega_1-\omega_2$ and $2\omega_2-\omega_1$, from the BPD can be expressed as

$$C_{2\omega_1-\omega_2} = 2J_{12}J_{02}\sqrt{R_1}\left[\sqrt{R_2}J_{21}J_{01} - \sqrt{R_0}J_{21}J_{01} - \sqrt{R_0}J_{11}J_{11}\right]$$
$$+ 2\sqrt{R_2}J_{12}J_{22}\left[\sqrt{R_3}J_{21}J_{01} - \sqrt{R_1}J_{11}J_{11}\right] + 2\sqrt{R_1}\sqrt{R_0}J_{01}J_{21}J_{12}J_{22} \qquad (13)$$

$$C_{2\omega_2-\omega_1} = 2J_{11}J_{01}\sqrt{R_1}\left[\sqrt{R_2}J_{22}J_{02} - \sqrt{R_0}J_{22}J_{02} - \sqrt{R_0}J_{12}J_{12}\right]$$
$$+ 2\sqrt{R_2}J_{11}J_{21}\left[\sqrt{R_3}J_{22}J_{02} - \sqrt{R_1}J_{12}J_{12}\right] + 2\sqrt{R_1}\sqrt{R_0}J_{11}J_{21}J_{02}J_{22} \qquad (14)$$

where $R_i(\omega)$ is the power spectral response of the OBPF for the frequencies of the optical carrier and the sidebands, as shown in Fig. 2. They are $R_0(\omega)$ for $\omega_1 - \omega_2$, ω_c, $\omega_2 - \omega_1$; $R_1(\omega)$ for $2\omega_1 - \omega_2$, ω_1, ω_2, $2\omega_2 - \omega_1$, $R_2(\omega)$ for $2\omega_1$, $\omega_1 + \omega_2$, $2\omega_2$, and $R_3(\omega)$ for $2\omega_1 + \omega_2$, $2\omega_2 + \omega_1$.

Assuming the modulation indexes for ω_1 and ω_2 are equal, $m_1 = m_2 = m$, the Bessel function can be written as $J_{n1}(m_1) = J_{n2}(m_2) = J_n(m)$. Using the approximation for the Bessel function, $J_0(m) \approx 1$, $J_1(m) \approx m/2$, and $J_2(m) \approx m^2/8$, Equations. (13) and (14) can be rewritten as

$$C_{2\omega_1-\omega_2} = C_{2\omega_2-\omega_1} = \frac{m^3}{8}\sqrt{R_1}\left[\sqrt{R_2}\left(1 - \frac{m^2}{4} + \frac{m^2}{8}\frac{\sqrt{R_3}}{\sqrt{R_1}}\right) - \sqrt{R_0}\left(3 - \frac{m^2}{8}\right)\right] \qquad (15)$$

From Eq. (15), it can be seen that in order to eliminate the IMD3 components, the term in the square bracket should be zero. When m is small enough, the terms of m^2 in the bracket of Eq. (15) could be neglected, and the condition for the elimination of the IMD3 components, $2\omega_1-\omega_2$ and $2\omega_2-\omega_1$, is

$$\alpha = \frac{R_2}{R_0} \approx 3^2 = 9 \approx 9.54\text{dB} \qquad (16)$$

Table 1. Fundamental components ω_1 and ω_2 of the output microwave signals from the BPD

Fundamental (ω_1)					
k-p = 1		l-q = 0		Coefficient	Derivation
k	p	l	q		
2	1	−1	−1	$2\sqrt{R_0 R_1}J_{21}J_{11}J_{-12}J_{-12}$	$(2\omega_1\text{-}\omega_2)\text{-}(\omega_1\text{-}\omega_2)$
		0	0	$2\sqrt{R_1 R_2}J_{21}J_{11}J_{02}J_{02}$	$(2\omega_1)\text{-}(\omega_1)$
		1	1	$2\sqrt{R_2 R_3}J_{21}J_{11}J_{12}J_{12}$	$(2\omega_1+\omega_2)\text{-}(\omega_1+\omega_2)$
1	0	0	0	$2\sqrt{R_0 R_1}J_{11}J_{01}J_{02}J_{02}$	(ω_1)
		1	1	$2\sqrt{R_1 R_2}J_{11}J_{01}J_{12}J_{12}$	$(\omega_1+\omega_2)\text{-}\omega_2$
		2	2	$2\sqrt{R_2 R_3}J_{21}J_{11}J_{12}J_{22}$	$(\omega_1+2\omega_2)\text{-}(2\omega_2)$
0	−1	1	1	$2\sqrt{R_0 R_1}J_{01}J_{-11}J_{12}J_{12}$	$(\omega_2)\text{-}(\omega_2\text{-}\omega_1)$
		2	2	$2\sqrt{R_1 R_2}J_{01}J_{-11}J_{22}J_{22}$	$(2\omega_2)\text{-}(2\omega_2\text{-}\omega_1)$
−1	−2	2	2	$2\sqrt{R_0 R_1}J_{-11}J_{-21}J_{22}J_{22}$	$(2\omega_2\text{-}2\omega_1)\text{-}(2\omega_2\text{-}\omega_1)$

Fundamental (ω_2)					
k-p = 0		l-q = 1		Coefficient	Derivation
k	p	l	q		
−1	−1	2	1	$2\sqrt{R_0 R_1}J_{-11}J_{-11}J_{22}J_{12}$	$(2\omega_2\text{-}\omega_1)\text{-}(\omega_2\text{-}\omega_1)$
0	0			$2\sqrt{R_1 R_2}J_{01}J_{01}J_{22}J_{12}$	$(2\omega_2)\text{-}(\omega_2)$
1	1			$2\sqrt{R_2 R_3}J_{11}J_{11}J_{22}J_{12}$	$(2\omega_2+\omega_1)\text{-}(\omega_2+\omega_1)$
0	0	1	0	$2\sqrt{R_0 R_1}J_{01}J_{01}J_{12}J_{02}$	ω_2
1	1			$2\sqrt{R_1 R_2}J_{11}J_{11}J_{12}J_{02}$	$(\omega_1+\omega_2)\text{-}\omega_1$
2	2			$2\sqrt{R_3 R_2}J_{21}J_{21}J_{12}J_{02}$	$(2\omega_1+\omega_2)\text{-}2\omega_1$
1	1	0	−1	$2\sqrt{R_0 R_1}J_{11}J_{11}J_{02}J_{-12}$	$\omega_1\text{-}(\omega_1\text{-}\omega_2)$
2	2			$2\sqrt{R_1 R_2}J_{21}J_{21}J_{02}J_{-12}$	$2\omega_1\text{-}(2\omega_1\text{-}\omega_2)$
2	2	−1	−2	$2\sqrt{R_0 R_1}J_{21}J_{21}J_{-12}J_{-22}$	$(2\omega_1\text{-}2\omega_2)\text{-}(2\omega_1\text{-}\omega_2)$

Table 2. IMD3 components ($2\omega_1$-ω_2) and ($2\omega_2$-ω_1) of the output microwave signals from the BPD

IMD3 ($2\omega_1$-ω_2)					
k-p = 2		l-q = −1		Coefficient	Derivation
k	p	l	q		
2	0	−1	0	$2\sqrt{R_0 R_1}\,J_{21}J_{01}J_{-12}J_{02}$	($2\omega_1$-ω_2)
		0	1	$2\sqrt{R_1 R_2}\,J_{21}J_{01}J_{02}J_{12}$	($2\omega_1$)-(ω_2)
		1	2	$2\sqrt{R_2 R_3}\,J_{21}J_{01}J_{12}J_{22}$	($2\omega_1 + \omega_2$)-$2\omega_2$
1	−1	0	1	$2\sqrt{R_0 R_1}\,J_{11}J_{-11}J_{02}J_{12}$	(ω_1)- (ω_2-ω_1)
		1	2	$2\sqrt{R_1 R_2}\,J_{11}J_{-11}J_{12}J_{22}$	($\omega_1 + \omega_2$) -($2\omega_2$-ω_1)
0	−2	1	2	$2\sqrt{R_1}\sqrt{R_0}\,J_{01}J_{-21}J_{12}J_{22}$	(ω_2) -($2\omega_2$-$2\omega_1$)
IMD3 ($2\omega_2$-ω_1)					
k-p = −1		l-q = 2		Coefficient	Derivation
k	p	l	q		
−1	0	2	0	$2\sqrt{R_0 R_1}\,J_{-11}J_{01}J_{22}J_{02}$	($2\omega_2$-ω_1)
0	1			$2\sqrt{R_1 R_2}\,J_{01}J_{11}J_{22}J_{02}$	($2\omega_2$)-(ω_1)
1	2			$2\sqrt{R_2 R_3}\,J_{11}J_{21}J_{22}J_{02}$	($2\omega_2 + \omega_1$)-($2\omega_1$)
0	1	1	−1	$2\sqrt{R_0 R_1}\,J_{01}J_{11}J_{12}J_{-12}$	(ω_2)-(ω_1-ω_2)
1	2			$2\sqrt{R_1 R_2}\,J_{11}J_{21}J_{12}J_{-12}$	($\omega_1 + \omega_2$)-($2\omega_1$-ω_2)
1	2	0	−2	$2\sqrt{R_1}\sqrt{R_0}\,J_{11}J_{21}J_{02}J_{-22}$	(ω_1) -($2\omega_1$-$2\omega_2$)

3. Experimental results

To verify that the proposed MPL is effective in the suppression of the even-order and the third-order distortions, a proof-of-concept experiment based on the system shown in Fig. 1 is implemented. A continuous-wave (CW) light at 1549.776 nm from a TLS (Yokogawa AQ2201) is sent to a PolM (Versawave, V_π = 5 V, 40 GHz) via PC1. The polarization direction of the light wave incident to the PolM is adjusted by PC1 to have an angle of 45° relative to one principal axis of the PolM. Two RF signals generated by a vector network analyzer (VNA, Agilent E8364) and a signal generator (SG, Agilent E8254A) are combined through an electrical coupler and sent to the PolM. The complementarily phase-modulated signals along the two principal axes of the PolM are then sent to the OBPF (Finisar WaveShaper 4000S). The left sidebands of the phase-modulated signals are suppressed by the OBPF to get the SSB + C signals. After being amplified by the EDFA (Nortel FA17UFAC), the SSB + C signals are sent to the PBS via PC2. By adjusting PC2, the two polarization principal axes of the PolM are aligned with those of the PBS. The two orthogonally polarized SSB + C signals are demultiplexed and fed to the BPD (Discovery Semiconductors, DSC740) through the two optical input ports. Two electrical signals are obtained at the outputs of PD1 and PD2 in the BPD and a differential signal is obtained at the output of the BPD, which is measured by an electrical spectrum analyzer (ESA, Agilent E4448).

3.1 Even-order distortion suppression

The even-order distortion suppression of the proposed MPL, and the performance comparison with a conventional MPL based on phase modulation and direct detection are conducted. For

the even-order distortions, the transmission performance of the MPL is mainly affected by the second harmonic of the lower-frequency fundamental signal on the higher frequency fundamental signal, for example, $2f_1$ on f_2 if $2f_1 \approx f_2$, and the second-order intermodulation component on the lower-frequency fundamental signal, for example, f_2-f_1 on f_1. Therefore, a two-tone RF signal with two frequencies of f_1 = 10 GHz and f_2 = 19.95 GHz is chosen to demonstrate the even-order distortion suppression. The two-tone RF signal with an identical power is applied to the PolM via the RF port. In the experiment, the conventional MPL is realized by aligning the polarization direction of the light wave from the TLS along one principle axis of the PolM and one principle axis of the PBS, and the optical power at the output of the EDFA is controlled identical to that of the proposed MPL. An SSB + C signal from one output port of the PBS is sent to one optical input port of the BPD. The electrical spectra of the detected RF signals at the output of the BPD are measured by the ESA.
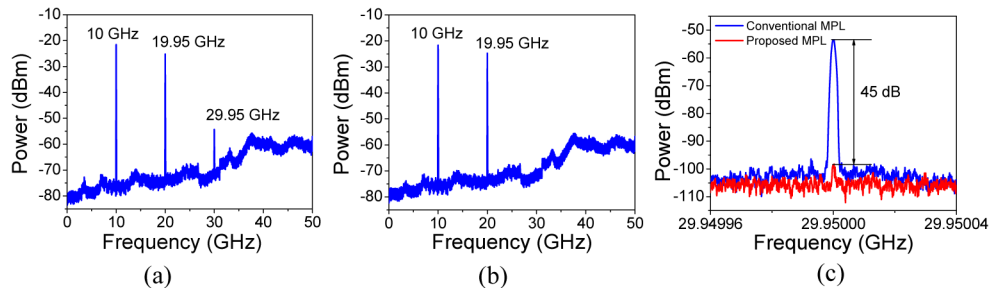
Fig. 3. Electrical spectra of the detected RF signals when a two-tone RF signal at 10 and 19.95 GHz is applied. (a) Conventional MPL; (b) proposed MPL; (c) the comparison of the IMD2 (f_1 + f_2)

First, we measure the spectra of the output RF signals for both the proposed MPL and the conventional MPL. The power for each of the two input RF signals is set at 5 dBm. Figure 3(a) shows the output electrical spectrum from the conventional MPL, measured by the ESA with a resolution bandwidth (RBW) of 100 kHz. As can be seen, a strong IMD2 (f_1 + f_2 = 29.95 GHz) component with a power as high as −54.3 dBm is observed. The output power at f_2 that is relatively lower than that at f_1 is due to the lower responsivity of the PDs at higher frequencies and also a greater loss of the RF cable at higher frequencies. Figure 3(b) shows the output electrical spectrum from the proposed MPL. As can be seen, no visible IMD2 component (f_1 + f_2 = 29.95 GHz) is observed in the spectrum. Figure 3(c) shows a zoom-in view of the spectra for both the proposed MPL and the conventional MPL, monitored by the ESA with a RBW of 50 Hz and a span of 100 kHz. It can be seen that a suppression ratio of the IMD2 (f_1 + f_2 = 29.95 GHz) as high as 45 dB is obtained.
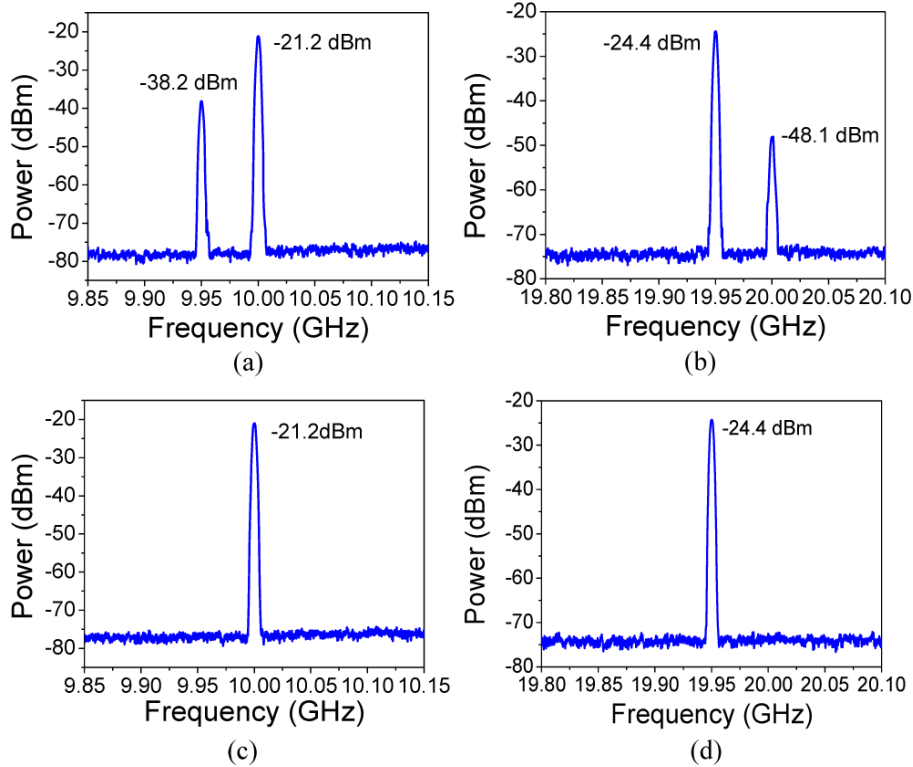
Fig. 4. Zoom-in view of the electrical spectra of the detected RF signals when a two-tone RF signal f_1 = 10 GHz and f_2 = 19.95 GHz is applied. (a) At 10 GHz and (b) at 19.95 GHz for the conventional MPL; (c) at 10 GHz and (d) at 19.95 GHz for the proposed MPL.

The SHD ($2f_1$) and the IMD2 (f_2-f_1) are more important in a practical system because they locate near the target signals ($2f_1 \rightarrow f_2, f_2$-$f_1 \rightarrow f_1$) and would degrade the performance of the MPL. Figures 4(a) and 4(b) give the zoom-in view of the electrical spectra around 10 and 19.95 GHz for the conventional MPL. The strong IMD2 (f_2-f_1 = 9.95 GHz, −38.2 dBm) and SHD ($2f_1$ = 20 GHz, −48.1 dBm) exist near the target RF components for the conventional MPL. Figures 4(c) and 4(d) show the zoom-in view of the electrical spectra from the proposed MPL. As can be seen, the IMD2 (f_1 + f_2 = 29.95 GHz, f_2-f_1 = 9.95 GHz) and SHD ($2f_1$ = 20 GHz) components are fully suppressed, and no visible IMD2 are shown. The measured electrical spectrum results demonstrate the effectiveness of the proposed MPL in suppressing the even-order distortions.
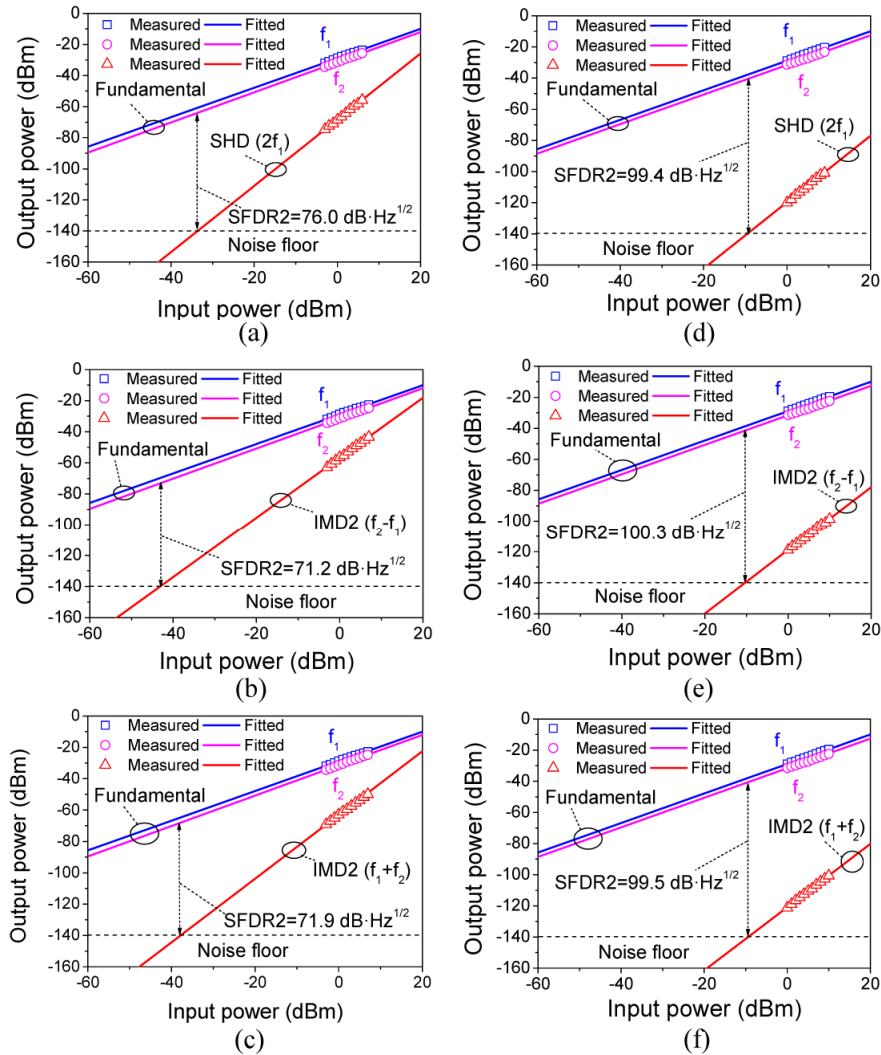
Fig. 5. The measured powers of the fundamental and the even-order components when a two-tone RF signal of f_1 = 10 GHz and f_2 = 19.95 GHz is applied. (a) SHD ($2f_1$), (b) IMD2 (f_2-f_1) and (c) IMD2 ($f_1 + f_2$) for the conventional MPL; (d) SHD ($2f_1$), (e) IMD2 (f_2-f_1) and (f) IMD2 ($f_1 + f_2$) for the proposed MPL.

The SFDR is an important performance measure for an MPL, which describes the range of the RF signal power that can be accommodated, taking into account the effects of the link noise and nonlinear distortions. We measure the output power of the target components and the even-order distortion components at different input RF power levels. The SFDR2 for both the proposed MPL and the conventional MPL are obtained by linear fitting the measured output powers of the fundamental and even-order distortion components. Figures 5(a)–5(c) show the measured and fitted results for the conventional MPL. The SFDR2 for the second harmonic ($2f_1$), the second intermodulation (f_2-f_1 and $f_1 + f_2$) are 76.0, 71.2 and 71.9 dB·Hz$^{1/2}$, respectively, for a noise floor of −140 dBm/Hz. Figures 5(d)–5(f) show the measured and fitted results for the proposed MPL. The SFDR2 for the second harmonic ($2f_1$), the second intermodulation (f_2-f_1 and $f_1 + f_2$) are 99.4, 100.3 and 99.5 dB·Hz$^{1/2}$, respectively, for a same noise floor of −140 dBm/Hz. The SFDR2 is enhanced by 23.4 dB for the second harmonic ($2f_1$), and 29.1 and 27.6 dB for the second intermodulation (f_2-f_1 and $f_1 + f_2$).

Note that the improvement in SFDR2s of the conventional MPL is different for SHD2 ($2f_1$), IMD2 (f_2-f_1) and IMD2 ($f_1 + f_2$), since the SFDR2s of the conventional MPL are different at different frequencies, because the responsivity of the PD for a low frequency is higher than that for a higher frequency. Thus, the SFDR2 for IMD2 (f_2-f_1 = 9.95 GHz) is lower than those for SHD2 ($2f_1$ = 20 GHz) and IMD2 ($f_1 + f_2$ = 29.95 GHz). While the SFDR2s of the proposed MPL are basically equal at different frequencies owing to the elimination of the even-order distortion by the balanced differential detection.

3.2 IMD3 suppression

According to the analysis in Section 2.2, the IMD3 can be suppressed when the spectral response of the OBPF meets the conditions given in Eq. (16). It can be achieved by optimizing the central wavelength and the bandwidth of the OBPF to make the wavelength of the optical carrier from the TLS to be located properly at the edge of the filter spectral response of the OBPF. Note that the IMD3 suppression is realized independently at each PD of the BPD by optimizing the spectral response of the OBPF, which does not affect the even-order distortion suppression although the frequency of the second fundamental signal is changed for the demonstration of the third order intermodulation suppression. In the experiment, the wavelength of the optical carrier is 1549.776 nm, and the central wavelength and the 3-dB bandwidth of the OBPF are 1550.320 nm and 1 nm, respectively. It makes the conditions in Eq. (16) be met and the MPL is applicable for broadband RF signal transmission. Figures 6(a) and 6(b) show the optical spectra of a phase-modulated signal before and after the OBPF. The left sideband is filtered out by the OBPF and a SSB + C signal is obtained. The optical carrier is partially suppressed, which is 9.54 dB lower than the right sideband, as expressed in Eq. (16). At the same time, the partial suppression of the optical carrier is helpful to increase the gain of the MPL when an EDFA is used to maintain the optical power to the BPD be a constant [21]. Note again that the partial suppression of the optical carrier along the two orthogonal polarization directions by the OBPF is identical, which does not affect the suppression of the second-order distortions.

To demonstrate the feasibility of the proposed MPL to suppress the IMD3 and to improve the SFDR3, a two-tone RF signal of 9.95 and 10 GHz with an identical power is fed to the PolM via the RF port. The reason to choose these two frequencies is that the transmission performance of the MPL is mainly affected by the third-order intermodulation component on the fundamental signals, for example, $2f_1$-f_2 on f_1 and $2f_2$-f_1 on f_2 if $f_1 \approx f_2$. However, since the suppression of the second-order distortions and the IMD3 are two independent processes, the use of these frequencies will not affect the suppression of the second-order distortions. The optical power to each optical input port of the BPD is fixed at 3.5 dBm by controlling the output power of the EDFA. A conventional MPL without optimizing the central wavelength of the OBPF is also measured as a comparison with the optimized MPL. In the experiment, the central wavelength of the OBPF in the conventional MPL is 1550.258 nm, which makes the wavelength of the optical carrier located at the top of the OBPF spectral response. The output electrical spectra from the conventional MPL and the optimized MPL are measured and the results are shown in Fig. 7(a) and (b), respectively, with a power of 5 dBm for each of the two input RF signals to the PolM. From Fig. 7(a) it can be seen that strong IMD3 components ($2f_1$-f_2 = 9.90 GHz and $2f_2$-f_1 = 10.05 GHz) are generated for the conventional MPL, and the carrier-to-interference ratio (CIR) is 30.8 dB. For the optimized MPL, as shown in Fig. 7(b), the CIR is more than 49.3 dB. The improvement in the CIR of 18.5 dB is achieved. Note that the spectral peaks in Fig. 7(b) are slightly wider than those in Fig. 7(a), which is caused due to the use of a wider span when measuring the spectrum shown in Fig. 7(b).
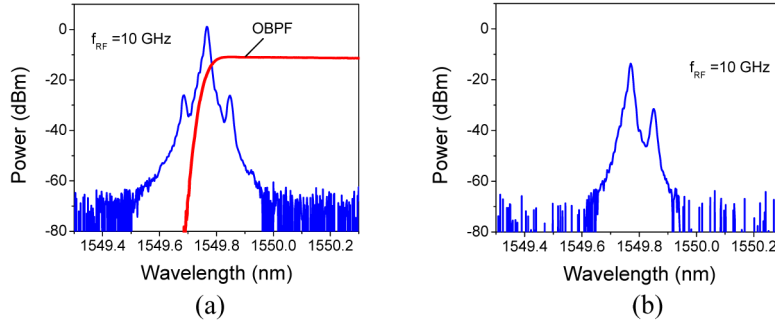
Fig. 6. Measured optical spectra of a phase-modulated modulated signal (a) before and (b) after the OBPF.
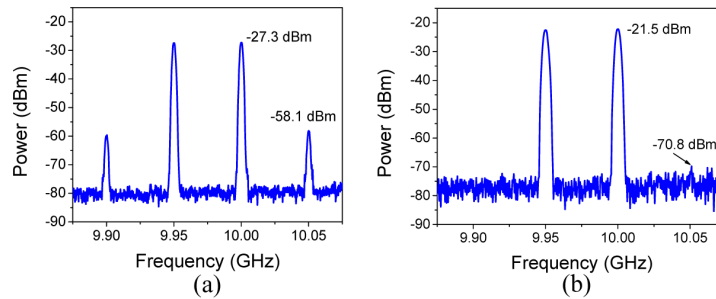
Fig. 7. Electrical spectra of the detected microwave signals when a two-tone RF signal of f_1 = 9.95 GHz and f_2 = 10 GHz is applied to the PolM. (a) A conventional MPL, and (b) an optimized MPL.
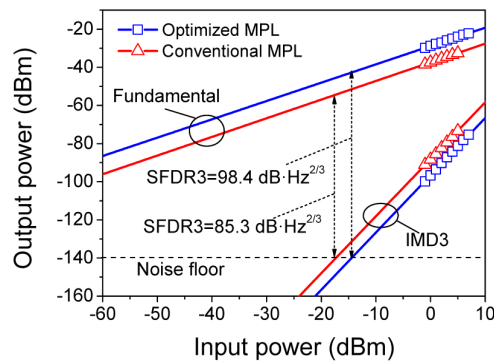
Fig. 8. Measured microwave powers of the fundamental and the IMD3 terms when a two-tone signal of f_1 = 9.95 GHz and f_2 = 10 GHz is applied.

The SFDR3 performance for both the conventional MPL and the optimized MPL is then measured and the results are shown in Fig. 8. For the conventional MPL, the SFDR3 is 85.3 dB·Hz$^{2/3}$ for a noise floor of −140 dBm/Hz. For the optimized MPL, the SFDR3 is 98.4 dB·Hz$^{2/3}$ for an identical noise floor of −140 dBm/Hz. As can be seen, the improvement of the SFDR3 is 13.1 dB. There are two factors that contribute to the improvement in SFDR3. One is the decrease in the IMD3 power due to the optimized spectral response of the OBPF, and the other is the increase in the fundamental signal power due to a higher gain of the optimized MPL. The higher gain of the optimized MPL, as compared with the conventional MPL, is obtained through partial suppression of the optical carrier by the OBPF while maintaining a constant optical power to the BPD [21, 22]. Thus, the proposed MPL has less loss than the

MPL reported in [19]. This is an added advantage to the proposed MPL. The IMD3 suppression by the optimized spectral response of the OBPF in the experiment is implemented using a programmable optical filter (Finisar WaveShaper 4000S). The minimum resolution of the WaveShaper is 10 GHz, which is large such that the IMD3 suppression is not as good as desired. As a result, the first factor has less contribution to the improvement in SFDR3 than the second factor. If a programmable optical filter with a higher resolution is used [23], an optimized carrier attenuation can be achieved and a better suppression in IMD3 could be achieved.

By comparing the above measured results for SFDR2 and SFDR3, it can be seen that the dynamic range of the proposed MPL is third-order distortion limited. The dynamic range of the MPL can be further enhanced by using a high power handling BPD. It was reported that a PD with an input power greater 30 dBm is now available [24]. If such a BPD is used, the gain of the MPL can be greatly enhanced by increasing the optical power to the BPD, thus the dynamic range can be further increased.

4. Discussions

According to the theoretical analysis in Section 2, the proposed MPL can suppress the even-order distortions by using the orthogonal polarization modulation and balanced differential detection and the third-order distortions by optimizing the spectral response of the OBPF with an optimal power ratio between the optical carrier and the sidebands of the phase-modulated signals from the PolM. The two suppression processes are independent and can be implemented simultaneously.

For the even-order distortion suppression, there is no frequency limitation as long as the bandwidths of the PolM and the BPD are wide enough. For the third-order distortion suppression, the lower cut-off frequency will be limited by the edge roll-off of the spectral response of the OBPF. In order to suppress the IMD3, the power response of R_0 for the optical carrier ω_c and the frequency difference components $\omega_1 - \omega_2$ and $\omega_2 - \omega_1$, and R_2 for the second harmonic components $2\omega_1$, $\omega_1 + \omega_2$, and $2\omega_2$, should meet the relationship given by Eq. (16). While the power spectral response $R_1(\omega)$ for $2\omega_1 - \omega_2$, ω_1, ω_2, $2\omega_2 - \omega_1$, has a no influence on the implementation of IMD3 suppression. Generally, the second harmonic components are located at the top of the OBPF spectrum and the optical carrier and frequency difference components are at the edge of the OBPF spectrum. For simplicity, the optical carrier ω_c and frequency-doubled component $2\omega_1$ are considered. If the roll-off rate of the edge of the OBPF spectrum is S (dB/GHz), the available lower cut-off frequency should be $f_L = \alpha/S/2$ GHz according to Eq. (16). For example, the roll-off rate of the OBPF in the experiment (Finisar WaveShaper 4000S) is $S = 1.2$ dB/GHz (150 dB/nm at 1550 nm), and the lower frequency is about 4 GHz. When the OBPF with a sharper roll-off edge is used, for instance, a waveguide chip based OBPF with a roll-off rate of about 12 dB/GHz [25], the lower cut-off frequency can be substantially decreased to 0.4 GHz, and the overall frequency range of the proposed MPL can be extended.

The proposed scheme can be generalized for a multi-tone signal. For example, when a three-tone signal at ω_1, ω_2 and ω_3 is applied to the proposed MPL, with a similar analysis in Section 2.1 and Section 2.2, the even-order distortions can be suppressed by using orthogonal polarization modulation and balanced differential detection, and the third-order distortions, including $2\omega_1-\omega_2$, $2\omega_2-\omega_1$, $2\omega_3-\omega_1$, $2\omega_1-\omega_3$, $2\omega_2-\omega_3$, $2\omega_3-\omega_2$, $\omega_1 + \omega_2-\omega_3$, $\omega_1 + \omega_3-\omega_2$ and $\omega_2 + \omega_3-\omega_1$, can be suppressed by optimizing the spectral response of the OBPF with the same power ratio, as expressed in Eq. (16), between the optical carrier and the sidebands of the phase-modulated signals from the PolM.

5. Conclusion

An MPL that is able to simultaneously suppress the even-order and third-order distortions has been proposed and experimentally demonstrated. The MPL was implemented using a single wavelength light source, a single PolM, an OBPF, an EDFA, a PBS and a BPD, which was much simpler compared with the previously reported MPLs. The fundamental concept to

achieve the simultaneous suppression of the even-order and third-order distortions was the use of orthogonal polarization modulation and balanced differential detection, to fully cancel the even-order distortion, and at the same time, the minimization of the third-order distortion by controlling the power ratio between the optical carrier and the sidebands of the phase-modulated signals from the PolM, which was done by optimizing the spectral response of the OBPF. An enhancement in SFDR2 by 23.4 dB for the second harmonic ($2f_1$), and 29.1 and 27.6 dB for the second intermodulation (f_2-f_1 and $f_1 + f_2$) has been obtained, as compared with a conventional MPL. An improvement in SFDR3 by 13.1 dB has been achieved, as compared with a conventional MPL.

Acknowledgments